Q-Band Resonance Raman Spectra of Oxidized and Reduced Mitochondrial bc_1 Complexes†

F. Gao,‡ H. Qin,§ D. B. Knaff,§ L. Zhang,|| L. Yu,|| C. A. Yu,|| and M. R. Ondrias*,‡

Department of Chemistry, University of New Mexico, Albuquerque, New Mexico 87131, Department of Biochemistry and Molecular Biology, Oklahoma State University, Stillwater, Oklahoma 74078-3035, and Department of Chemistry and Biochemistry, Texas Tech University, Lubbock, Texas 79409-1061

Received January 9, 1998; Revised Manuscript Received April 22, 1998

ABSTRACT: Recently published crystallographic studies of mitochondrial bc_1 complexes have stimulated renewed interest in the active site architecture of these important integral membrane proteins. We present resonance Raman spectra obtained via variable excitation within the heme Q-band from samples poised in several different net redox states. Appropriate subtraction and polarization analysis allows the vibrational behavior of the individual heme b_L, b_H, and c_1 sites to be assessed. The spectra of the b hemes are particularly noteworthy. They exhibit evidence for a protonation equilibrium involving heme axial ligands and reveal a marked structural heterogeneity at the heme b_H site that most likely involves nonplanar distortions of the macrocycle. The possible implications of these findings for heme functionality are discussed.

The cytochrome bc_1 complexes comprise a superfamily of integral membrane proteins, which plays a pivotal role in the electron-transport chains of mitochondria, chloroplasts, and bacteria. They catalyze the flow of electrons from two-electron donors (quinol) to one-electron acceptors (soluble *c* cytochromes or plastocyanin) and actively pump protons across their host membrane (*1*−*3*). The modified Q-cycle (*4*) is now accepted as the general mechanism for transferring reducing equivalents within bc_1 complexes. However, despite years of intensive study, the detailed molecular mechanisms for the various electron-transfer pathways and the coupling of proton translocation to the exogenicity of the electron-transfer reactions remain largely unknown.

While all bc_1 complexes contain a core of three redox-active proteins, harboring a total of four redox-active sites (three hemes and one FeS cluster), the net subunit composition of the complex varies with organism. Bacterial bc_1 complexes generally contain few or no additional protein subunits (*3, 5*). In contrast, bovine heart mitochondrial bc_1 complex consists of 11 protein subunits (*6, 7*). The additional subunits have been implicated in structural and regulatory roles within the complex (*2*).

A recent X-ray diffraction study has produced atomic-scale models of most protein components of bc_1 complexes from bovine heart mitochondria (*8*). These show that the crystallized oxidized cytochrome bc_1 complex exits as a dimer. Each monomer is anchored in the membrane by 13 transmembrane helices. Eight of these belong to cytochrome *b*. A large protein region composed primarily of core proteins 1 and 2 and subunits 6 and 7 extends far (∼75 Å) into the matrix. Two much smaller regions consisting of cytochrome c_1 and the iron−sulfur protein are located in the intermembrane space.

During the past 2 decades, much has been learned concerning the structural and functional properties of the redox-active prosthetic groups in bc_1 complexes (*9*−*16*). Each monomer has three heme centers which are redox active during the catalytic cycle. In mitochondrial bc_1 complexes, the midpoint redox potentials for heme b_H, heme b_L, and heme c_1 are ∼90 mV, ∼−30 mV, and ∼225 mV, respectively (*17*). All three hemes are six-coordinate and low-spin. The specific amino acid side chains serving as ligands for the b_H and b_L hemes are four conserved histidines lying within transmembrane helices B and D. The results of near-infrared MCD[1] (*18, 19*), EPR (*18, 20*), and mutagenesis (*5, 9, 21*) studies are all consistent with this assignment. The recent crystal structure models confirmed the coordination of His^{97} and His^{196} to heme b_H, and His^{83} and His^{182} to heme b_L (*8*). The His/Met axial ligation for cytochrome c_1 inferred by earlier studies (*14, 17*) was also confirmed in the crystallographic data.

Despite their qualitative similarities, the *b* hemes exhibit distinct spectroscopic and electrochemical behavior. The structural details giving rise to these differences remain a subject of debate. Most important for the present study is the fact that the local environments of the *b* hemes produce a small variation in their electronic absorption spectra. This is most evident in the α-band. Optically monitored redox

† This work is supported by NIH Grants (GM33330 (to M.R.O.) and GM 30721 (to C.A.Y.), by U.S.D.A. Grant 93-37306-9084 (to D.B.K.), and by Robert A.Welch Foundation Grant D-0710 (to D.B.K.).

‡ University of New Mexico.

§ Texas Tech University.

|| Oklahoma State University.

[1] Abbreviations: RR, resonance Raman; RRS, resonance Raman spectroscopy; MCD, magnetic circular dichroism; EPR, electron paramagnetic resonance; UV−Vis, ultraviolet−visible absorption spectroscopy; CCD, charged couple device; EDTA, ethylenediaminetetraacetic acid; r.c.; *Rhodobacter capsulatus*; Rb., *Rhodobacter*; FePP-$(ImH)_2$, iron protoporphyrin bisimidazole; Im^-, imidazolate.

S0006-2960(98)00065-8 CCC: $15.00
Published on Web 06/13/1998

titrations (*22*) have shown that for a wide range of bacterial and mitochondrial bc_1 complexes, the b_H hemes consistently exhibit α-bands that are blue-shifted relative to their b_L counterparts (558−562 vs 565 nm). Careful studies of mitochondrial bc_1 by Howell and Robertson have revealed further inhomogeneous broadening of the b_L heme α absorption band (*22*).

Resonance Raman spectroscopy (RRS) has proven to be a reliable probe of the structural characteristics of chromophores in proteins (*23*). It is particularly useful for assessing the local environments of active heme sites (most notably heme axial ligation and direct protein environment/heme interactions) and, in principle, provides a direct means to further characterize the local structure and function of the individual heme sites in bc_1 complexes. However, resonance Raman studies of bc_1 heme sites are complicated by the qualitative similarity of their absorption spectra. For example, excitation into the Soret absorption band produces heme vibrational spectra with strongly overlapping contributions from all three hemes. In contrast, the small differences in the α-band maxima of the hemes permit some resonance selectivity in their Raman scattering using 540−570 nm excitation. Our recent study of the bc_1 complex from *Rb. capsulatus* demonstrated that individual heme spectra could be analyzed by employing a combination of redox manipulation and variable excitation wavelength within the composite heme α-band absorption (*24*). In the present study, we extend these techniques to examine the individual structures of the hemes in bovine heart mitochondrial bc_1 complexes.

MATERIALS AND METHODS

Cytochrome bc_1 and cytochrome c_1 were isolated from bovine heart and *Rb. capsulatus*, purified via previously described methods (*25*, *26*), and stored in liquid nitrogen until needed. All other chemicals were obtained from commercial sources and were the highest purity available. Samples of monomeric complexes were produced by Centricon-30 buffer exchange with an appropriate buffer solution (20 mM Tris-HCl, 1 mM EDTA, 1.0 M NaCl, and 0.1 g/mL Tween 20 at pH 7.5), following the method of Musatov and Robinson (*27*).

The bc_1 purification protocol produced samples with a mixture of $c_1(+2/+3)$ redox states, and they were further treated to manipulate the net redox state of the hemes. Fully oxidized (all ferric hemes), partially reduced [$c_1(+2)$ $b_H(+2)$-$b_L(+3)$], and fully reduced (all ferrous hemes) samples were prepared by the addition of minimal amounts of solid potassium ferricyanide, sodium ascorbate, and sodium dithionite, respectively, to solutions of bc_1 complexes buffered to a pH of 8.0 (in 50 mM Tris-HCl, 100 mM NaCl, 0.1 mg/mL dodecyl maltoside solutions).

Ten nanosecond pulses generated by a Molectron DL-14 dye laser pumped by a UV-24 nitrogen pulsed laser were used as a Raman excitation source. The system is tunable from 390 to 800 nm and operates at a repetition rate of about 10−15 Hz. The excitation beam was line-focused onto the sample by a cylindrical lens and a prism. The scattered light was collected by using backscattering geometry (∼135° from the excitation beam) and passed through a polarization scrambler and appropriate long-pass filters to reduce stray light background before being focused on the entrance slit of a Chromex (Albuquerque, NM) 500IS spectrograph equipped with a liquid N_2 cooled (−100 °C) CCD detector. A Model ST-135 detector controller interfaced with a PC (16 MB RAM) was used for data collection. Chromsoft software was used to control the data acquisition and initial data processing. Subsequent data manipulation is described further in the appropriate figure captions.

Raman experiments were conducted with cells specially constructed to maximize signal reproducibility, while minimizing sample volume. These consisted of truncated glass pipets with the narrow end sealed and the other end capped with airtight septa. Adapters were designed to hold the cells in fixed positions for reproducible alignment in both Raman and UV−Vis instruments. Anaerobic conditions were achieved by purging the stoppered cells with nitrogen gas. Reducing agents were introduced into the deoxygenated sample through airtight septa by Hamilton syringes. The net redox states and overall integrity of the samples were monitored by absorption spectroscopy before and after the Raman experiments.

RESULTS

Absorption Spectra. Figure 1 displays the Q-band absorption spectra of relevant mitochondrial bc_1 species. The absorption spectrum for the isolated ferrous cytochrome c_1 subunit is typical of *c*-type cytochromes. Spectra of the sodium ascorbate- and dithionite-reduced bc_1 complexes reflect the difference in the redox potentials of the two *b* hemes. The addition of ascorbate to ferric mitochondrial bc_1 complexes (Figure 1, trace Ib) produces two α-bands (at ∼552 and ∼562 nm) arising from ferrous hemes c_1 ($E°$ ∼225 mV) and b_H ($E°$ ∼90 mV). The b_L heme in mitochondrial bc_1 complex has a potential of ∼−30 mV and remains ferric. Addition of a small amount of sodium dithionite ($E°' = -527$ mV) reduces all three hemes, producing additional absorption at ∼560 to ∼565 nm from ferrous b_L (trace Ic).

Appropriate subtraction of traces I(c) and II(a), II(b) reveals a marked splitting of the heme b_L α-band. The two maxima (at ∼565 and 558 nm) reproduce the behavior reported by Howell and Robertson (*22*) for mitochondrial cytochrome bc_1 and previously observed for the *Rb. capsulatus* bc_1 complex.

Resonance Raman Spectra. The distinct α absorption bands for the individual hemes in the bc_1 complex can be exploited to separate and characterize their individual vibrational properties via resonance Raman spectroscopy. Scattering intensities are strongly dependent on the resonance conditions between the excitation light and heme optical transitions (*23*). Thus, spectra obtained from fully reduced bc_1 complexes with 550 nm excitation are dominated by scattering from heme c_1, while 560 and 565 nm excitation preferentially enhances scattering from the *b* hemes (*24*).

Since ferric hemes do not contribute significantly to spectra obtained with 550−565 nm excitation, the individual contributions from ferrous hemes can be further separated by manipulating the net redox state of the sample. Ascorbate-reduced complexes exhibit scattering from ferrous c_1, and b_H only, while spectra from dithionite-reduced species contain contributions from all three hemes. Figure 2 shows the dependence of the mitochondrial bc_1 spectra upon the net redox state of the complex and excitation wavelengths in

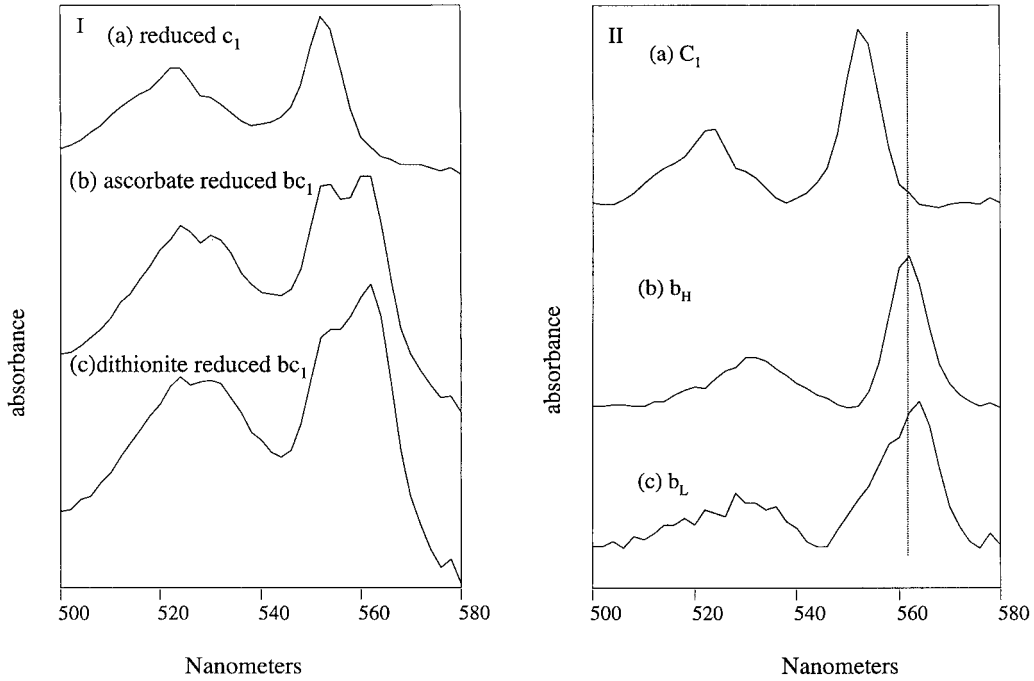

FIGURE 1: Q-band region absorption spectra of bovine heart mitochondrial bc_1 complexes and isolated subunits. (Panel I) (a) Ferrous c_1 subunit, (b) bc_1 complex immediately after addition of ascorbate; (c) ferrous bc_1 complexes reduced with dithionite (see Materials and Methods for experimental details). The bc_1 and isolated c_1 samples were in a buffer of 50 mM phosphate, pH 7.4. All samples were ~150 μM in protein. (Panel II) Base line corrected and isolated spectra for individual hemes: (a) heme c_1, base line corrected spectra of I(a); (b) heme b_H, smoothed spectra of I(b) − I(a); (c) heme b_L, smoothed spectra of Ic − IIa − IIb.

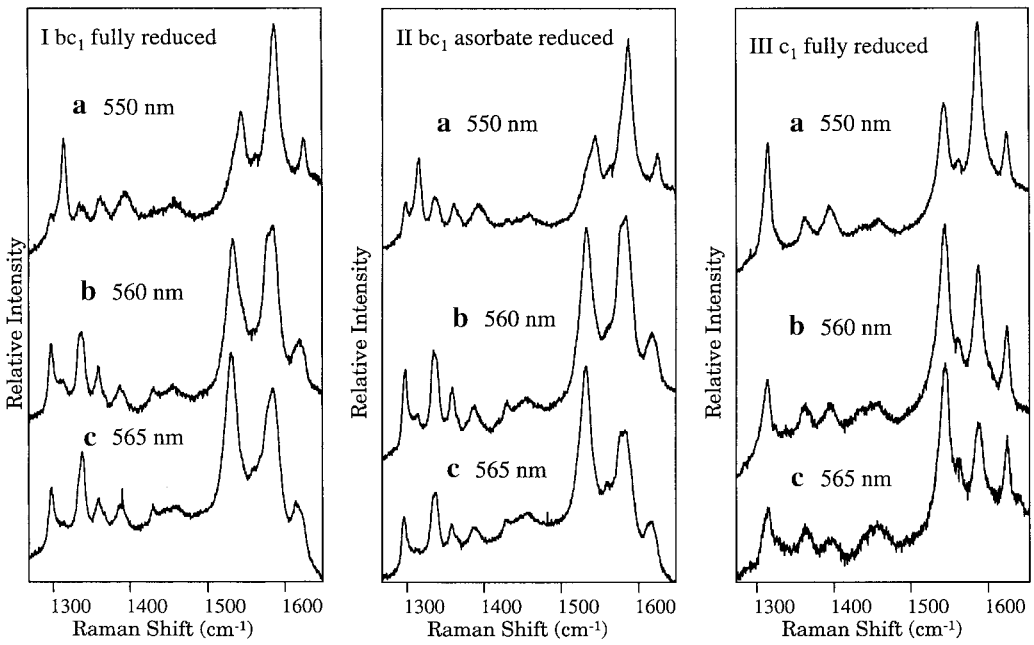

FIGURE 2: Q-band resonance Raman spectra of bovine heart mitochondrial bc_1 complexes and isolated c_1 subunits. (Panel I) Spectra of ferrous bc_1 ($c_1$2+, b_H2+, b_L2+) complexes obtained with (a) 550 nm, (b) 560 nm, and (c) 565 nm excitation. (Panel II) Spectra of ascorbate-reduced bc_1 ($c_1$2+, b_H2+, b_L3+) complexes at (a) 550 nm, (b) 560 nm, and (c) 565 nm excitation. (Panel III) Spectra of ferrous c_1 subunits at (a) 550 nm, (b) 560 nm, and (c) 565 nm excitation Sample preparation was the same as Figure 1 with a protein concentration of ~150 μM. Laser power of ~8 mW at 10 Hz was used. Long-pass wavelength filters, SOG-570 and LP-580 (CVI Laser, Albuquerque), were used to minimize background. Spectra were accumulated for 6−10 min at a spectral resolution of ~4 cm^{-1}.

the α region (550−565 nm). The ferrous c_1 subunit displays only heme c_1 modes which decrease in absolute intensity as the excitation wavelength is increased from 550 to 565 nm. In contrast, spectra of dithionite- and ascorbate-reduced bc_1 complexes show a marked dependence on the excitation wavelength. The relative contributions of heme c_1 to these spectra are reflected in the intensities of the vinyl thioether mode at ~1320 cm^{-1}, which splits into bands at 1300 and 1340 cm^{-1} for hemes *b* (*28*). It is apparent that while 550 and 560 nm excitation yields spectra that are a mixture of c_1 and *b* modes, spectra obtained with 565 nm excitation are completely dominated by heme *b* modes. A closer comparison of spectra from ascorbate- and dithionite-reduced complexes (Figure 3) reveals that spectra of the *b* hemes are not identical. As expected, spectra of the ascorbate-reduced complex (c_1(2+), b_H(2+), b_L(3+)) are very

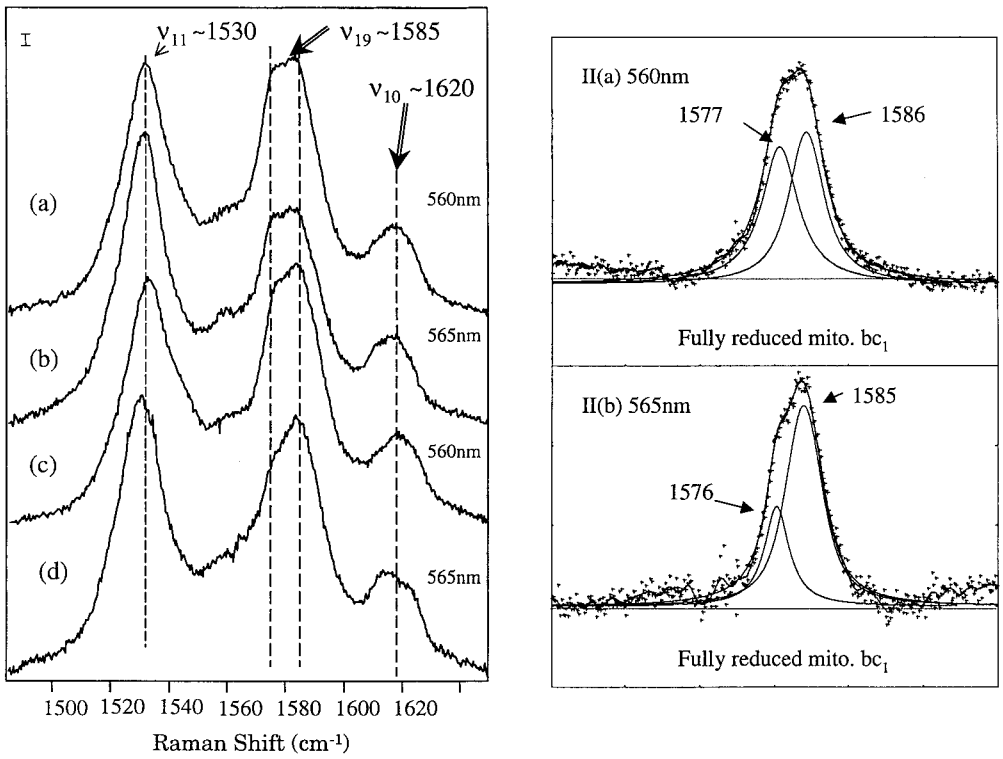

FIGURE 3: High-frequency Q-band RR spectra of bovine heart mitochondrial bc_1 complex in various net oxidation states. (Panel I) (a) Ascorbate-reduced bc_1 complex (c_1(2+), b_H(2+), b_L(3+)), at 560 nm excitation [same as Figure 2II(b)]; (b) ascorbate-reduced bc_1 complex (c_1(2+), b_H(2+), b_L(3+)), at 565 nm excitation [same as Figure 2II(c)]; (c) dithionite-reduced bc_1 complex ($c_1$2+, b_H2+, b_L2+), at 560 nm excitation [same as Figure 2I(b)]; (d) dithionite-reduced bc_1 complex (c_1(2+), b_H(2+), b_L(2+)), at 565 nm excitation [same as Figure 2I(c)]. (Panel II) Polarization analysis of the high-frequency spectra from fully reduced bc_1 complexes. Spectra are derived from the weighted subtraction of perpendicular polarized spectra from parallel polarized spectra sufficient to remove all depolarized bands. (a) 560 nm excitation; (b) 565 nm excitation. For details of the curve-fitting procedure, see ref *40*.

Table 1: Summary RR Modes for Fully Reduced Mitochondrial bc_1 Complex and c_1 Subunit Obtained with Q-Band Excitation

	composite spectra				isolated heme spectra		
mode	c_1 550 nm	bc_1 550 nm	bc_1 560 nm	bc_1 565 nm	c_1	b_H	b_L
$\delta_{(CH=)}$(cm^{-1}), ap		1297	1297	1297		1297	1298
ν_{21}(cm^{-1}), ap	1314	1314	1314		1314		
$\delta_{(=CH_{2(2)})}$(cm^{-1}), ap		1335	1335	1337		1335	1338
$\delta_{(CH_3)}$(cm^{-1}), dp	1362	1363	1359	1359	1362	1358	1360
(?)ν_{29}(cm^{-1}), dp	1394	1395	1387	1387	1394	1385	1389
ν_{11}(cm^{-1}), dp	1544	1544	1532	1530	1544	1531	1528
ν_{19}(cm^{-1}), ap	1587	1587	1577, 1584	1577, 1584	1587	1577, 1583	1580, 1586
ν_{10}(cm^{-1}), dp	1624	1624	1620	1614, 1622	1624	1616	1614,1623

similar at the two excitation wavelengths. In contrast, comparable spectra of the dithionite-reduced complex (all ferrous hemes) reflect the increased level of b_L contributions at the longer excitation wavelength. The position of ν_{11} (~1530 cm^{-1}) shifts noticeably as the relative contributions of b_L and b_H are varied. In addition, all four spectra display composite peaks in the ν_{19} region (~1580 cm^{-1}), but there are large wavelength-dependent changes in the net band shapes only for the dithionite-reduced species.

The B_g and A_{2g} modes which dominate heme Q-band scattering are easily distinguished by their polarizations (depolarized and anomalously polarized, respectively) (*23*). Since ν_{19} is the sole A_{2g} mode in the 1500−1650 cm^{-1} region, it can be isolated by the appropriate subtraction of parallel and perpendicular polarized spectra (see Figure 3 caption). The results of such an analysis are shown in Figure 3II. It is clear that the multicomponent nature of the band at ~1585 cm^{-1} arises solely from heterogeneity in ν_{19}.

Spectra of the individual hemes can be isolated by the judicious subtraction of the net spectra of the isolates $c_1$2+, $c_1$2+/b_H2+/b_L3+ (ascorbate-reduced), and $c_1$2+/b_H2+/b_L2+ (dithionite-reduced) species (see figure caption for details). These are summarized in Table 1. The "isolated" spectra of b_H and b_L clearly show that there are pronounced differences in both the position of ν_{11} and the band shapes of ν_{19} and ν_{10} for these species. Here again a polarization analysis can be employed to isolate ν_{19} (Figure 4II). Both *b* hemes exhibit heterogeneity in their ν_{19} band shapes, but b_H displays a far more prominent low-energy component. Note also that the band at 1560 cm^{-1} in the b_L absolute spectrum is depolarized and thus is not an additional component of ν_{19}.

High-quality spectra for the oxidized bc_1 and dissociated c_1 subunits were also obtained. To our knowledge, these represent the first spectra of an oxidized bc_1 complex obtained with Q-band excitation. Figure 5 and Table 2

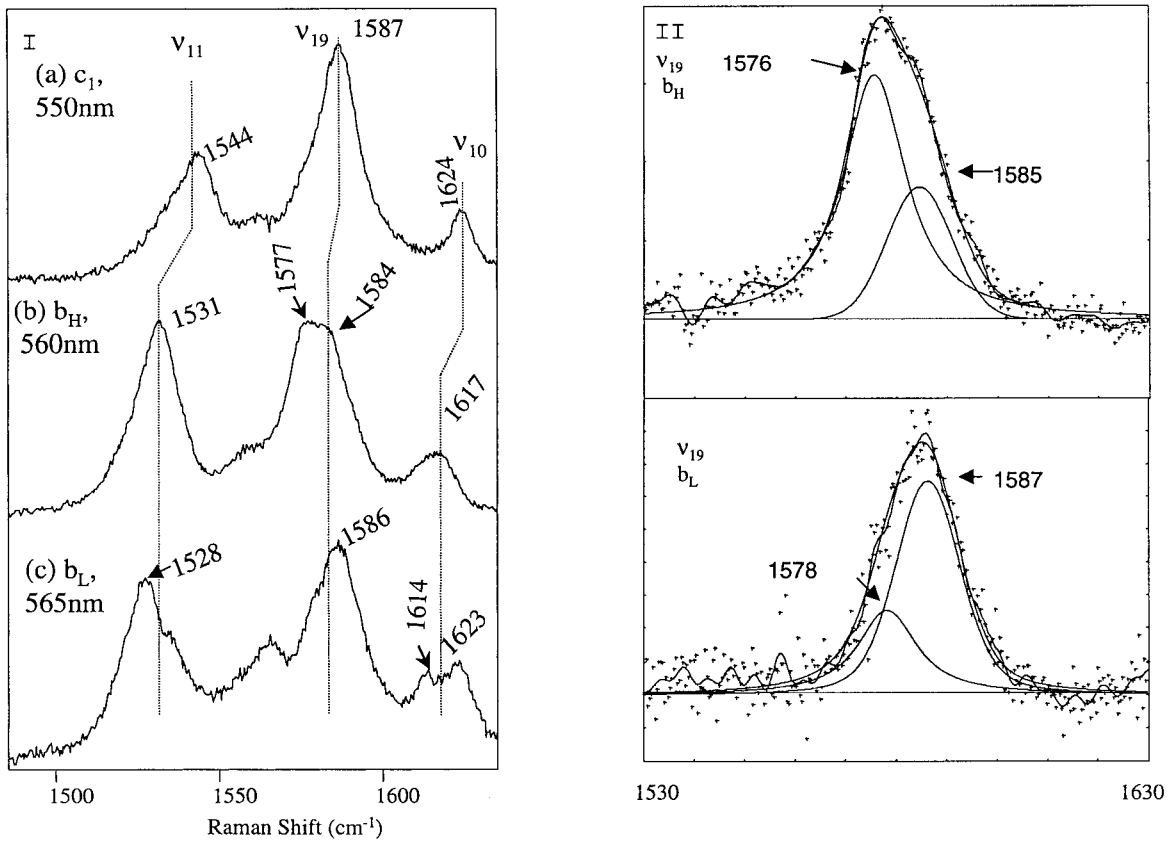

FIGURE 4: Isolated Q-band RR spectra (base line corrected) for ferrous bc_1 hemes. (Panel I) (a) c_1 subunit (550 nm); (b) ferrous heme b_H spectrum (560 nm) obtained by the weighted subtraction of the ferrous c_1 subunit spectrum at 560 nm [Figure 2III(b)] from the ascorbate-reduced bc_1 spectrum at 560 nm [Figure 2II(b)]; (c) ferrous heme b_L spectrum at 565 nm excitation obtained by subtracting the ascorbate-reduced bc_1 spectrum [2II(c)] from the dithionite-reduced bc_1 spectrum [2I(c)]. (Panel II) Decomposition and curve-fitting results for isolated ν_{19} from polarization data, as per procedures described in ref *40*. (a) Isolated heme b_H; (b) isolated heme b_L.

Table 2: Summary RR Modes for Bovine Heart Mitochondrial bc_1 Complex and c_1 Subunit Obtained with 540 nm Excitation

mode	oxidized c_1	reduced c_1	oxidized bc_1	ascorbate-reduced bc_1	dithionite-reduced bc_1
$\delta_{(CH=)}$(cm^{-1})			1302	1297	1298
ν_{21}(cm^{-1})	1317	1314	1317	1314	1314
$\delta_{(=CH_{2(2)})}$(cm^{-1})			1343	1338	1338
$\delta_{(CH_3)}$(cm^{-1})	1370	1363	1370	1359	1360
(?)ν_{20}(cm^{-1})	1406	1395	1399	1388	1387
ν_{11}(cm^{-1})	1564	1544	1564	1532, 1544	1530
ν_{19}(cm^{-1})	1589	1587	1585	1585	1585
$\nu_{(C=C)}$(cm^{-1})			1620		
ν_{10}(cm^{-1})	1640	1624	1640	1640	1623

summarize these results. For the c_1 subunit, the heme redox change is most evident in the pronounced shifts of the positions of ν_{11} and ν_{10}. Redox-dependent changes are also evident in spectra of the complex. In particular, the oxidized complex exhibits an ~5 cm^{-1} upshift in the vinyl mode at ~1340 cm^{-1}. This may be used as a marker for the net oxidation state of the *b* hemes. Redox-induced effects can also be seen in the band shape for ν_{19} for 540 nm excitation, the large shifts and intensity increase for the ν_{10} (~1640 cm^{-1}) and ν_{11} (~1560 cm^{-1}) of heme c_1, and the growth of a heme *b* vinyl mode at ~1620 cm^{-1} in spectra of the oxidized complex. Unfortunately, both oxidation states of all three hemes contribute significantly to spectra observed with 520−540 nm excitation, and thus resonance selectivity cannot be used to further isolate the individual heme behavior.

DISCUSSION

Cytochrome c_1. The RR spectra of the dissociated ferrous and ferric bovine heart mitochondrial c_1 subunit (Figures 3III and 5, respectively) are quite similar to those of c_1 cytochromes from other bc_1 complexes (*17*) and smaller soluble cytochromes *c* (see Table 1). The position and relative intensities of the high-frequency modes are entirely consistent with the methionine/histidine heme axial ligation inferred from previous spectroscopic (*17*−*19*) and crystallographic studies (*8*). Some small variability in the position of ν_{11} among the c_1 spectra of *Rb. capsulatus* c_1, mitochondrial c_1, and *Rb. sphaeroides* c_1 suggests that minor differences may exist in the heme pocket environments of these species.

Spectra of the reduced bc_1 complexes obtained with 550 nm excitation are dominated by heme c_1 scattering except for the *b* heme ν_{21} and vinyl modes at ~1300 and ~1340 cm^{-1}, respectively. The positions, line shapes, and relative intensities of the prominent high-frequency modes (ν_{11}, ν_{19}, and ν_{10}) are virtually identical to those in spectra of the dissociated ferrous c_1 subunit. This strongly suggests that the structure of the c_1 active site is not influenced by other subunits in the complex. Given the isolation of the c_1 subunit from the membrane-spanning and core-protein subunits and its exposure to the mitochondrial intermembrane space (*8*), this insensitivity is not surprising.

Axial Ligation of b Hemes. The most direct heme−protein interactions occur via the coordination of amino acid residues to the two vacant axial octahedral sites of the heme iron. Based upon genetic (*5*, *9*, *21*), spectroscopic (*17*, *18*), and

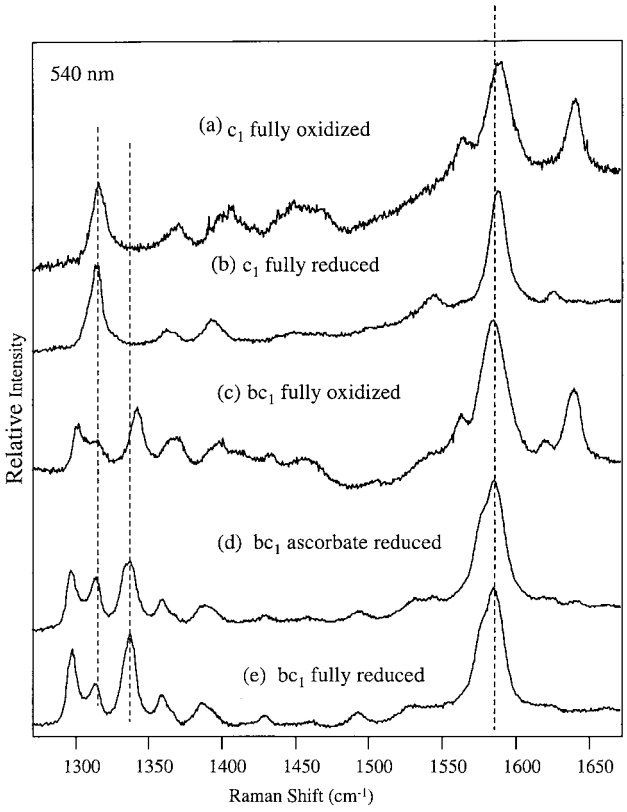

FIGURE 5: 540 nm excitation (Q-band) RR spectra of bovine heart mitochondrial bc_1 species. (a) Isolated c_1, fully oxidized; (b) isolated c_1, fully reduced; (c) bc_1, fully oxidized; (d) bc_1, ascorbate reduced; (e) bc_1, dithionite reduced. Sample preparations were the same as Figure 1 with a protein concentration of ~150 μM. For the oxidized species, the spectra were accumulated for 15 min; for the reduced species, the spectra were accumulated for 5−6 min.

crystallographic (*8*) evidence, the axial ligation of both *b* hemes can be assigned as bishistidine. However, variation within this general motif can produce functionally important structural differences.

ν_{11} (~1520−1545 cm^{-1}) is the high-frequency mode most sensitive to axial ligand influences. Many studies (*29*−*33*) have demonstrated that the position of ν_{11} is influenced by π back-donation from axial ligands to the iron $e_g(d_\pi)$ and porphyrin $e_g(\pi^*)$ orbitals, In general, the frequency of ν_{11} decreases with ligand electron donor strength.

The behavior of ν_{11} in Figures 3 and 4 strongly suggests that details of the bishistidyl ligation differ for hemes b_H and b_L. For the composite spectra, ν_{11} shifts to lower frequency as the excitation is tuned for a stronger resonance (565 nm) with heme b_L. The "isolated" spectra (Figure 4) clearly show that the frequency of ν_{11} is 3 cm^{-1} higher for b_H vs b_L in mitochondrial bc_1 complexes.

A comparison of spectra from mitochondrial and bacterial (*Rb. capsulatus*) complexes reveals interspecies variation in the behavior of ν_{11} (see Figure 6). In this case, the positions of ν_{11} in both composite and "isolated" spectra are uniformly lower for the mitochondrial complex. Furthermore, the difference between heme b_H and heme b_L is less dramatic in the mitochondrial ($\Delta\upsilon = 3$ cm^{-1}) than in the bacterial ($\Delta\upsilon = 8$ cm^{-1}) complex.

A study by Debois and Lutz (*32*) revealed that within a series of heme imidazole derivative complexes, the position of ν_{11} could be directly related to the protonation state of

Scheme 1

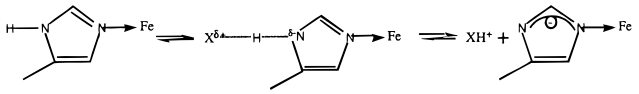

the axial ligands. For the iron−protoporphyrin model compounds Fe(II)PP(ImH)$_2$, Fe(II)PP(ImH)(Im^-), and Fe(II)PP(Im^-)$_2$, ν_{11} decreases by about 15 cm^{-1}, reflecting the increased donor strength of the imidazolate ion.

We conclude that the variability of ν_{11} in heme *b* spectra most likely arises from the partial deprotonation (or strong H-bonding) of at least one of the axial histidines of heme b_L in both complexes and of heme b_H in the mitochondrial species. This would require specific heme *b* environments that simultaneously lower the pK_a of at least one axial imidazole and provide nearby nucleophiles for proton abstraction or H-bonding. Such protein control of the cytochrome active site is not unprecedented. Indeed, H-bonding networks involving heme ligands have been implicated in maintaining the heme pocket architecture during redox transitions in soluble cytochromes. Recent modeling studies by Howell and co-workers provide a more specific picture of possible heme−protein interaction for the heme *b* sites. In particular, the distances of the histidine N_1 nitrogen from the heme iron atom and the orientation of the histidine imidazole planes are controlled principally by the number of amino acid residues between the ligand pairs, by the relative orientation of the two helical protein segments, and by the hydrogen bonding of the N_3 nitrogen of the histidine ligands to the protein backbone.

The strength of axial ligand H-bonding interactions would be quite sensitive to the local heme pocket geometry, and thus the equilibrium positions of the deprotonation reaction in Scheme 1(and hence the position of ν_{11}) would be expected to vary among heme *b* species. Our data suggest that deprotonation/H-bonding interactions are more pronounced at the heme b_L sites for both mitochondrial and bacterial bc_1 complexes. Furthermore, the deprotonation equilibrium for the b_H sites seems poised further to the right for the mitochondrial species than for the bacterial complexes. To the extent that imidazole deprotonation is connected (via a network of proton donor/acceptors) to protonation dynamics at the nearby Q_o site, it may provide a direct coupling mechanism for electron transfer and proton pumping within the complex.

Conformational Heterogeneity of the b Hemes. Another obvious difference in the spectra of bacterial and mitochondrial bc_1 complexes lies in the band shapes of ν_{19} (~1585 cm^{-1}) and ν_{10} (~1620 cm^{-1}) for b-type hemes. In contrast to the relatively narrow and symmetric band shapes exhibited by the *Rb. capsulatus* bc_1 complexes, the mitochondrial bc_1 spectra display band shapes and line widths which are suggestive of heterogeneous heme populations. In particular, the ν_{19} band is clearly composed of at least two overlapping bands. This heterogeneity cannot include contributions from c_1, since it is also obvious in the "isolated" spectra of the *b* hemes (Figure 4) where all c_1 contributions have been removed. Furthermore, the polarized spectra (Figure 3II) convincingly demonstrate that only anomalously polarized scattering from ν_{19} (the only ap mode in the 1550−1650 cm^{-1} region) contributes to the net band shape. Analysis of the polarized "isolated" spectra of hemes b_H and b_L (Figure

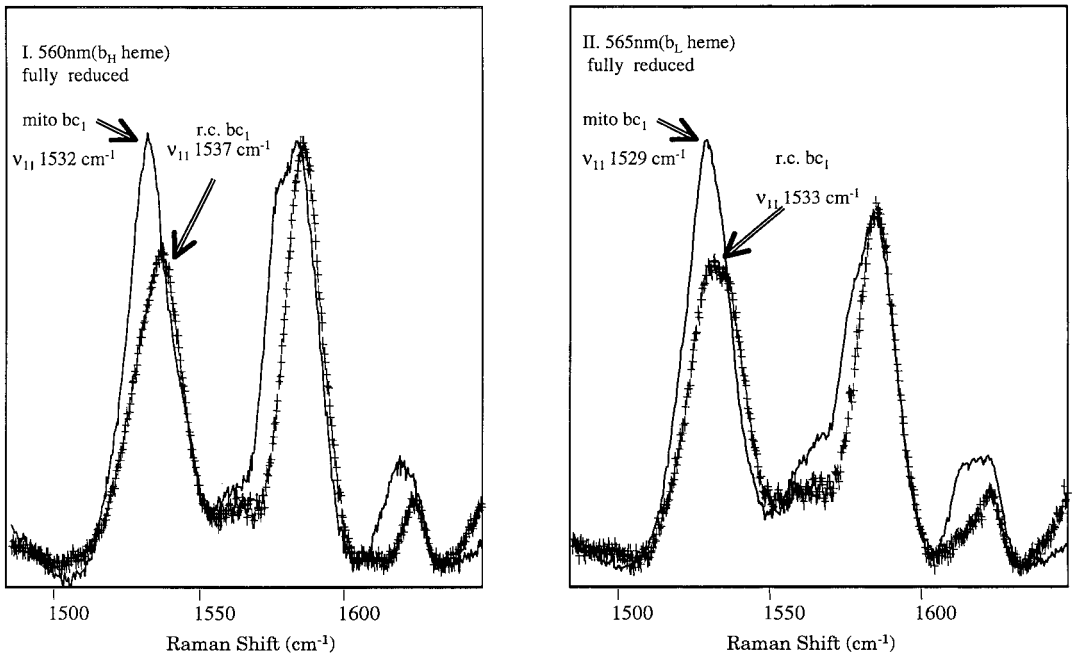

FIGURE 6: Comparison of the high-frequency region Q-band RR spectra of fully reduced bovine heart mitochondrial bc_1 and *Rb. capsulatus* bc_1 complexes. (a) 560 nm excitation; (b) 565 nm excitation. In both panels, the solid line is the spectrum for bovine heart bc_1 complex, and the plus line denotes the spectra of the r.c. bc_1 complex.

4II) confirms that both hemes experience heterogeneity in their local environments. Both spectra are best fit with two bands in the ν_{19} region. Heme b_H displays a larger composite line width (fwhm, 22 vs 17 cm^{-1}) and a much larger contribution from the lower energy component than heme b_L.

The relative insensitivity of ν_{19} and ν_{10} bands to axial ligand strength (*30*, *32*, *34*, *35*) suggests that axial ligation electronic effects are not the origin for the distinctive *b* heme populations. The likelihood of coupling between ligand protonation and conformational heterogeneity is further diminished by the fact that the *b* heme spectra of *Rb. capsulatus* bc_1 complexes exhibit similar ν_{11} behavior (and, by inference, axial ligand protonation) without evincing heterogeneity in ν_{19} and ν_{10}. Instead, the different heme populations most likely arise from protein-induced structural distortions of the heme macrocycle.

Shelnutt and co-workers have employed a combination of spectroscopic and computer modeling techniques to definitively characterize the nonplanar distortions of metalloporphyrin model compounds and heme protein active sites (*36*−*39*). In general, nonplanar distortions slightly decrease the on-plane π-bonding of the macrocycle and lower the frequency of selected in-plane vibrational modes. Of the high-frequency modes, ν_{19} and ν_{10} are particular sensitive to the distortion of heme planrity. A recent study of nickel(II) 5,15-disubstituted porphyrin by Song et al. showed that increasing distortion of the heme plane causes a proportional red shift in the Q_0 absorption spectrum and a decrease in the frequency of the ν_{19} and ν_{10} bands (*35*). Other high-frequency modes (most notably ν_{11}) showed much less sensitivity to heme distortions from planarity.

The magnitudes of the shifts of ν_{10} and ν_{19} for the *b* hemes are considerably smaller than those exhibited by the grossly distorted model systems. This observation coupled with the coexistence of at least two distinct conformers is consistent with the existence of structural equilibria involving modest distortion of heme planarity at these sites. Because of its distinctive polarization, the heterogeneity is more easily verified and quantified for ν_{19}. Figure 4II clearly shows that the effect is much more pronounced for heme b_H. Interestingly, the positions of the two ν_{19} components are nearly the same in b_H and b_L spectra, and their line widths are suggestive of two reasonably homogeneous subpopulations. Thus, it is likely that the structural equilibria at both heme sits involve two similar conformers. However, the equilibrium at heme b_H exhibits a larger population of the more distorted conformer.

Since the individual spectra of the ferric hemes could not be isolated via redox manipulation, analysis of heme *b* heterogeneity in the oxidized complex is qualitative at best. A composite spectrum of both *b* hemes can be produced by subtraction of the ferric c_1 and oxidized bc_1 spectra (Figure 5). Curve-fitting of the composite ν_{19} (not shown) reveals it to be narrower than the composite ν_{19} of the ferrous hemes (18 vs 20 cm^{-1}). This suggests a greater net heterogeneity in the ferrous hemes.

In an effort to determine whether dimerization could trigger long-range interactions affecting the *b* heme pockets and produce the spectral differences between mitochondrial and r.c. bc_1 complexes, spectra were obtained for fully reduced complexes under solution conditions (*27*) known to dissociate the dimers. These exhibited ν_{19} and ν_{10} line shapes that were nearly identical to those of the dimer (data not shown). This precludes dimerization as a determining factor in the heme *b* structural heterogeneity.

The available mitochondrial bc_1 crystal structure does not allow resolution of atomic positions within the cytochrome *b* heme pockets. Thus, the origin of heme *b* structural distortions remains speculative. Previous analyses of crystal structures of *c*-type cytochromes attribute the distortion of the heme plane to steric restrictions imposed by the covalent thioether linkage of the heme to protein cysteines or van der Waals contacts and hydrogen bonding within the heme

pocket. The first possibility is obviously not viable for the *b* heme sites. Thus, it appears that the multiple *b* heme conformers are induced by differences in nonbonding interactions with other residues within the heme pocket. It is unclear at this time whether these changes in local heme pocket contacts are predicated on more extensive structural equilibria within the complex.

SUMMARY AND CONCLUSIONS

The results of this study form the basis for a more detailed investigation of the structural and functional characteristics of the heme active sites in bc_1 complexes. The resonance Raman spectra of heme c_1 strongly suggest that it is a relatively typical *c*-type heme whose local environment is not influenced by the rest of the complex. In contrast, the heme *b* sites exhibit distinct spectra which indicate that their local environments directly affect both their structure and their function. The extent of axial ligand protonation clearly affects the electron density within the macrocycle and provides a means to modulate heme redox potential. Structural heterogeneity within the individual heme pockets is, to our knowledge, quite novel and not as readily interpreted. In any case, the *b* hemes (particularly b_H) clearly reside in structurally flexible protein environments which induce at least two energetically accessible conformers. It is tempting to speculate that these structural equilibria may be controlled by more global protein structural changes, and thus provide a means of long-range communication between redox sites in the complex.

ACKNOWLEDGMENT

We thank Songlin Jia and Dr. John A. Shelnutt for helpful discussions.

REFERENCES

1. Hauska, G., Hurt, E., Gabellini, N., and Lockau, W. (1983) *Biochim. Biophys. Acta 726*, 97−133.
2. Brandt, U., and Trumpower, B. L. (1994) *Crit. Rev. Biochem. Mol. Biol. 29*, 165−197.
3. Knaff, D. B. (1993) *Photosynth. Res. 35*, 117−133.
4. Mitchell, P. (1976) *J. Theor. Biol. 62*, 327−367.
5. Gennis, R. B., Barquera, B., Hacker, B., Van Doren, S. R., Arnaud, S., Crofts, A. R., Gray, K. A., and Daldal, F. (1993) *J. Bioenerg. Biomembr. 25*, 195−209.
6. Gonzalez-Halphen, D., Lindorfer, M. A., and Capaldi, R. A. (1988) *Biochemistry 27* (18), 7021−7031.
7. Schagger, H., Link, T. A., Engel, W. D., and von Jagow, G. (1986) *Methods Enzymol. 126*, 224−237.
8. Xia, D., Yu, C.-A., Kim, H., Xia, J.-Z., Kachurin, A. M., Zhang, L., Yu, L., and Deisenhofer, J. (1997) *Science 277*, 60−66.
9. Yun, C. H., Crofts, A. R., and Gennis, R. B. (1991) *Biochemistry 30*, 6747−6754.
10. Yun, C. H., Wang, Z., Crofts, A. R., and Gennis, R. B. (1992) *J. Biol. Chem. 267*, 5901−5909.
11. Robertson, D. E., Farid, R. S., Moser, C. C., Urbauer, J. L., Mulholland, S. E., Pidikiti, R., Lear, J. D., Wand, A. J., DeGrado, W. F., and Dutton, P. L. (1994) *Nature 368*, 425−432.
12. Hobbs, J. D., Kriaucuunas, A., Guner, S., Knaff, D. B., and Ondrias, M. R. (1990) *Biochim. Biophys. Acta 1018*, 47−54.
13. Hobbs, J. D., Wynn, M., Nunez, D. J., Malkin, R., Knaff, D. B., and Ondrias, M. R. (1991) *Biochim. Biophys. Acta 1059*, 37−44.
14. Gray, K. A., Davisdon, E., and Daldal, F. (1992) *Biochemistry 31*, 11864−11873.
15. Chen, Y. R., Shenoy, S. K., Yu, C. A., and Yu, L. (1995) *J. Biol. Chem. 270*, 11496−11501.
16. Beattie, D. S., Jenkins, H. C., and Howton, M. M. (1994) *Arch. Biochem. Biophys. 312*, 292−300.
17. Lou, B.-S., Hobbs, J. D., Chen, Y. -R., Yu, L., Yu, C. -A., and Ondrias, M. R. (1993) *Biochim. Biophys. Acta 1144*, 403−410.
18. Finnegan, M. G., Knaff, D. B., Qin, H., Gray, K. A., Daldal, F., Yu, L., Yu, C. A., Kleis-San Francisco, S., and Johnson, M. K. (1996) *Biochim. Biophys. Acta 1274*(1−2), 9−20.
19. Simpkin, D., Palmer, G., Devlin, F. J., Mckenna, M. C., Jensen, G. M., and Stephens, P. J. (1989) *Biochemistry 28*, 8033−8039.
20. Carter, K. R., Tsai, A., and Palmer, G. (1981) *FEBS Lett. 132*, 243−246.
21. Hauska, G., and Herrmann, R. G. (1988) *J. Bioeng. Biomembr. 20*, 211.
22. Howell, N., and Robertson, D. E. (1993) *Biochemistry 32*, 11162−11172.
23. Spiro, T. G., and Li, X. (1987) *Biol. Appl. Raman Spectrosc. 3*, 1−38.
24. Gao, F., Qin, H., Simpson, M. C., Shelnutt, J. A., Knaff, D. B., and Ondrias, M. R. (1996) *Biochemistry 35*(39), 12812−12819.
25. Yu, C. A., and Yu, L. (1980) *Biochim. Biophys. Acta 591*(2), 409−420.
26. Guner, S., Willie, A., Millett, F., Caffrey, M. S., Cusanovich, M. A., Robertson, D. E., and Knaff, D. B. (1993) *Biochemistry 32*, 4793−4800.
27. Musatov, A., and Robinson, N. C. (1994) *Biochemistry 33*(44), 13005−13012.
28. Kitagawa, T., Kyogoku, Y., Iizuka, T., Ikeda-Saito, M., and Yamanaka, T. (1975) *J. Biochem. 78*(4), 719−728.
29. Othman, S., Fitch, J., Cusanovich, M. A., and Desbois, A. (1997) *Biochemistry 36*(18), 5499−5508.
30. Othman, S., Le Lirzin, A., and Desbois, A. (1994) *Biochemistry 33*, 15437−15448.
31. Cartling, B. (1983) *Biophys. J. 43*(2), 191−205.
32. Desbois, A., and Lutz, M. (1992) *Eur. Biophys. J. 20*, 321−335.
33. Desbois, A. (1994) *Biochimie 76*(7), 693−707.
34. Othman, S., Richaud, P., Vermeglio, A., and Desbois, A. (1996) *Biochemistry 35*(28), 9224−9234.
35. Song, X. -Z., Jentzen, W., and Shelnutt, J. A. (1996) *J. Am. Chem. Soc. 118*(51), 12975.
36. Hobbs, J. D., and Shelnutt, J. A. (1995) *J. Protein Chem. 14* (1), 19−25.
37. Jentzen, W., Scheidt, W. R., and Shelnutt, J. A. (1996) *Inorg. Chem. 35*(12), 3559.
38. Jentzen, W., Song, X. -Z., and Shelnutt, J. A. (1997) *J. Phys. Chem. 101*(9), 1684.
39. Shelnutt, J. A., Medforth, C. J., and Berber, M. D. (1991) *J. Am. Chem. Soc. 113*(11), 4077.
40. Jentzen, W., Unger, E., Karvounis, G., Shelnutt, J. A., Derybrodt, W., and Schweitzer-Stenner, R. (1996) *Phys. Chem. 100* (33), 14184−14191.

BI9800653